Shallow donor muonium states in II-VI semiconductor compounds

J. M. Gil, H. V. Alberto, R. C. Vilão, J. Piroto Duarte, and N. Ayres de Campos
Physics Department, University of Coimbra, P-3004-516 Coimbra, Portugal

A. Weidinger and J. Krauser
Hahn-Meitner Institut Berlin, Glienicker Strasse 100, D-14109 Berlin, Germany

E. A. Davis
Department of Physics and Astronomy, University of Leicester, Leicester LEI 7RH, United Kingdom

S. P. Cottrell
ISIS Facility, Rutherford Appleton Laboratory, Chilton OX11 0QX, United Kingdom

S. F. J. Cox
ISIS Facility, Rutherford Appleton Laboratory, Chilton OX11 0QX, United Kingdom
and Physics Department, University College London, London WCE 6BT, United Kingdom
(Received 8 February 2001; published 26 July 2001)

Experimental data on shallow donor muonium states in the II−VI semiconductor compounds CdS, CdSe, CdTe, and ZnO are presented. These are characterized by very weak hyperfine interactions amounting to approximately 10^{-4} of the free-atom value, and by donor levels with binding energies comparable to those calculated on the hydrogenic model of the shallow centers. The data are discussed in terms of a model generalizing the knowledge of muonium and hydrogen states in tetrahedrally bonded semiconductors. Within this model the shallow muonium state is attributed to muonium bound to the anion of the II−VI compound and located at the antibonding site or close to it in the bond direction.

DOI: 10.1103/PhysRevB.64.075205 PACS number(s): 61.72.Vv, 71.55.Gs, 76.75.+i

I. INTRODUCTION

Interstitial hydrogen in semiconductors has been the subject of active research since the mid 1980s, when it was finally recognized as one of the most significant impurities affecting the evolving semiconductor technologies (for a recent review see Ref. 1). The muon spin rotation (μSR) and related techniques have contributed substantially to this field, pioneering the research as regards the isolated defect centers.[2–4] The relevance of the muon work here is that it exploits the similarity of the behavior of positive muons to protons and allows a unique spectroscopic characterization. Since the muons are observed with the highest possible dilution in the sample—often with only one of these particles present at a time—and since they usually have no time to find or pair with impurities before are observed with the highest possible dilution in the sample decaying, the muon is well suited to provide information on the intrinsic properties of interstitial hydrogen defect centers in semiconductors.

Extensive μSR data are available for Si and Ge and the III-V compounds.[2–4] A feature of the experiments is that the muons commonly pick up electrons on implantation at low temperature to form muonium ($\mathrm{Mu}=\mu^+e^-$) which mimics atomic hydrogen. The spin states are also sufficiently long lived (in intrinsic or lightly doped material) for the muonium sites and electronic structures to be established from the μSR spectra. Particularly important was the discovery of metastability of the neutral paramagnetic centers and identification of the bond-center site. Recent studies have turned attention to the charged defects, which we denote Mu^+ and Mu^-, mimicking the interstitial proton and hydride ion, and to the interplay of site and charge state that is relevant to the mobility and electrical activity of hydrogen. The situation now is that new types of wide-gap semiconductors, including the II−VI compounds, are on the verge of important applications. Defects and impurities are found to play particularly important roles in these new materials. While hydrogen is by no means the only such impurity, it is certainly one of the most significant, controlling the mechanism of deposition and doping and affecting final electronic properties. We have therefore initiated μSR studies on II−VI compounds and related chalcopyrites with a view to elucidate these questions and to obtain atomistic pictures of muonium and hydrogen behavior.[5–7] A surprising and quite unanticipated first result was the recent observation of a shallow muonium state in CdS.[5] A theoretical paper followed, predicting a shallow donor hydrogen state in ZnO as well.[8] We were able to confirm this prediction by spectroscopic observation of its muonium counterpart.[6] We present here a survey of these shallow states as found in several II−VI compound semiconductors, summarizing their properties and systematics.

The volume of data accumulated on the muon states in semiconductors—elemental group-IV, -III-V, and -II-VI compounds—suggests that some simple guidelines for the interpretation of the data may be useful. In silicon, the correspondence between muon and proton states, their energy levels and electrical activity, are quite well established,[9,10] so that muonium should serve as a guide to hydrogen behavior in the other materials also. We therefore propose a simple set of rules to help in discussing the interpretation of those diversified experimental data from common viewpoints. This

set of rules seeks to unify the various aspects discussed in the literature,[2–4,8,11] and goes beyond these by generalization to all tetrahedrally bonded semiconductors.

II. EXPERIMENTAL DETAILS

The μSR experiments were performed at the ISIS Facility, RAL, in the UK and at PSI in Switzerland. At ISIS we used, as a special arrangement, the so-called "fly-past" method,[12] where care is taken that muons that do not hit the sample are stopped far away from it and therefore do not contribute to a decay signal, rendering a virtually background-free spectrum. At PSI, the muons-on-request method was used on the GPS instrument in most cases. In this arrangement, the piM3 beam is interrupted after a muon stop has been detected in the sample.[13] The next muon is allowed to enter the sample only after a preselected time, usually about 20 μs. This also allows the recording of clean spectra and background-free data at long elapsed times. Since in the present studies good frequency resolution is required, measurements up to long times are essential.

The samples consisted mainly of commercially available undoped single crystals (from CrysTec) with an area of 1 to 2 cm^2 and a thickness of about 1 mm. The ZnO sample was polycrystalline with the highest-purity available (99.999%, from AlfaAesar). Conventional transverse- and longitudinal-field arrangements were used.[2–4] By measuring the decay positrons from muons implanted into the sample, the time development of the muon spin polarization is recorded. In the analysis of data, instead of the usual Fourier transform, in most cases we used a slightly modified transformation introduced by Lomb.[14] In this transformation, the lower statistics at long times in the muon decay may be taken into account. We found that the frequency spectrum becomes clearer with this analysis than with the usual Fourier transformation. In the case of the powder-pattern spectrum for ZnO the maximum entropy method was used.

III. RESULTS

Figure 1 shows muon spin-rotation signals recorded at ISIS at low temperature (4–5 K) for the four materials studied in these experiments. A beating is seen in all four signals, indicating the presence of more than one precession frequency. The nodes in the beating, which are an approximate measure of the frequency differences, vary from material to material. In Fig. 2 we show the corresponding frequency spectra. Basically, a three-line pattern is observed in each case. The central line corresponds to diamagnetic muons, i.e., it represents the Larmor precession of the muon spin in the external field. The symmetrically placed satellites on either side of the middle line are due to the hyperfine splitting in the muonium-state formed at these temperatures. That is, the hyperfine field either adds to or subtracts from the external field according to whether the electron spin is up or down. In the strong-field limit, the separation of the two lines gives the hyperfine constant directly.

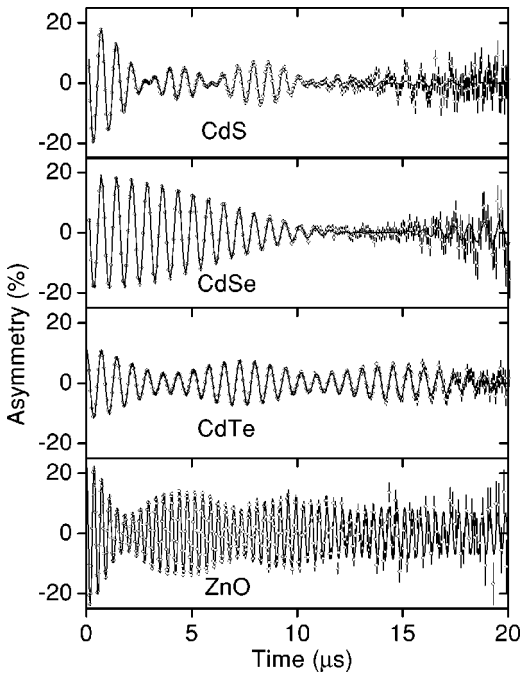

FIG. 1. μSR time spectra at low temperatures (4–5 K) in transverse field for the four compounds CdS, CdSe, CdTe, and ZnO. The field was $B=10$ mT in the case of the Cd compounds, and $B=20$ mT in the case of ZnO. The beating pattern originates from the splitting of precession frequencies, with a period related to the hyperfine constants of the paramagnetic muonium, i.e., of the undissociated donor. The solid lines are the results of fits with three precession frequencies. A large missing fraction of the amplitude is noticeable in the CdTe spectrum.

A. Hyperfine interaction parameters

In the case of an anisotropic interaction, the splitting changes with the angle between the axis of the hyperfine tensor and the direction of the external applied field. For axial symmetry, the anisotropic hyperfine tensor has principal elements $A_{\parallel}$, parallel to the symmetry axis, and $A_{\perp}$, perpendicular to this axis. An equivalent description of the hyperfine interaction expresses it as a combination of an isotropic and a traceless dipolar term. The isotropic part is given by $A_{\mathrm{iso}}=\frac{1}{3}(A_{\parallel}+2A_{\perp})$ whereas the dipolar tensor is described by the asymmetry parameter $D=\frac{2}{3}(A_{\parallel}-A_{\perp})$, yielding the hyperfine interaction A as a function of angle θ between the symmetry axis and the direction of the external field:

$$A=A_{\mathrm{iso}}+\frac{D}{2}(3\cos^2\theta-1). \tag{3.1}$$

This expression holds in the Paschen-Back region, already true here for fields of the order of 2 mT for Cd compounds and 5 mT for ZnO.

From orientation-dependent measurements on single crystals, both the hyperfine interaction parameters and the direction of the symmetry axis can be derived. For a polycrystalline sample, the principal values of the tensor are accessible but not the crystallographic direction of its symmetry axis, since this is oriented randomly relative to the external field, within the range of θ from 0 to $\pi/2$. As a consequence of this

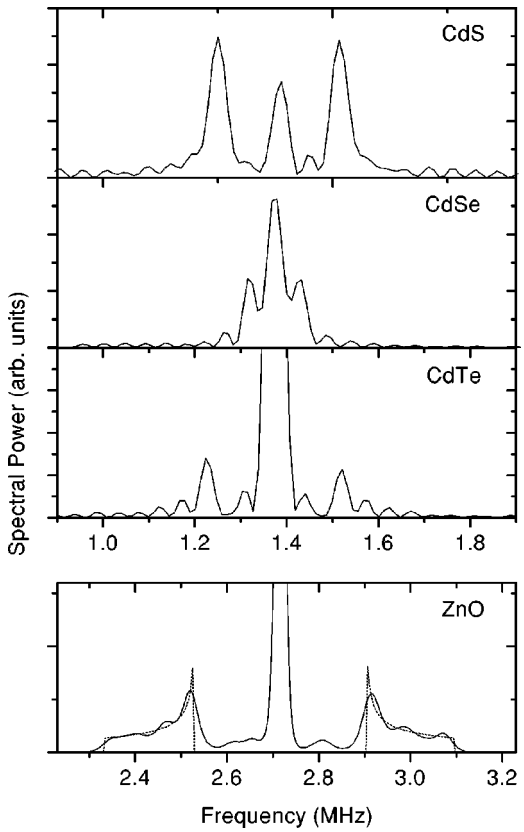

FIG. 2. Frequency-spectra derived from the time spectra of Fig. 1, for the compounds CdS, CdSe, CdTe, and ZnO. The central-line corresponds to the Larmor precession of the diamagnetic muon. The separation of the symmetrically placed satellites is a direct measure of the hyperfine interaction of the paramagnetic muonium. The anisotropy of the hyperfine tensor is seen as a powder-pattern broadening of the satellite lines in the case of polycystalline ZnO, where the dashed line is the predicted distribution.

random orientation, the observed splitting is composed of a frequency distribution, characterized by an average value ($A_{\rm iso}$) and a width (proportional to D). The following expression is derived for the normalized intensity of the distribution or "powder pattern" dI/dA:

$$\frac{dI}{dA}=\frac{dI}{d\theta}\frac{d\theta}{dA}=\frac{1}{\sqrt{3D}}\frac{1}{\sqrt{2(A-A_{\rm iso})+D}} \quad \text{for} \quad \left(A_{\rm iso}-\frac{D}{2}\right)\leqslant A\leqslant A_{\rm iso}+D. \tag{3.2}$$

The values obtained from the analysis of the time spectra of the four compounds are summarized in Table I. For CdS, the hyperfine anisotropy is determined in this manner and we find that the symmetry axis is along the Cd-S bond direction. Of the four bond directions, one is along the c axis direction, the other three are at 109.4° to it. Although these directions are not strictly equivalent, the data suggest that they are similarly populated. For CdSe and CdTe, orientation-dependent

TABLE I. Hyperfine parameters and Bohr radii for three tetrahedrally bonded Cd compounds and ZnO. $A_{\rm iso}=\frac{1}{3}(A_{\parallel}+2A_{\perp})$ is the isotropic part of the hyperfine interaction. The anisotropic part D is defined as $D=\frac{2}{3}(A_{\parallel}-A_{\perp})$, and is proportional to the difference between the hyperfine interaction parallel ($A_{\parallel}$) and perpendicular ($A_{\perp}$) to the symmetry axis, which is along the bond direction. The experimental Bohr radii $r_{\rm exp}$ were deduced from the ratio of $A_{\rm iso}/A_0$, where A_0 is the vacuum value. The theoretical Bohr radii $r_{\rm theo}$ are calculated in the hydrogenic model with the effective masses and dielectric constants of the individual materials (Ref. 15).

	CdS	CdSe	CdTe	ZnO
$A_{\rm iso}$ (kHz)	244(5)	87(4)	261(4)	500(20)
D (kHz)	91(6)	<40	<50	260(20)
$r_{\rm exp}$ (nm)	1.40	1.97	1.37	1.10
$r_{\rm theo}$ (nm)	2.4	3.9	6.2	1.7

measurements showed no changes in the frequencies within experimental error; thus only an upper limit for the D parameter can be given. For ZnO, the anisotropy is obtained from the powder distribution.

The values of the hyperfine interaction found are four orders of magnitude smaller than the vacuum-state muonium value of 4463 MHz. This huge reduction of the spin density of the electron at the muon site indicates that either major spin density is localized elsewhere or that it is distributed over many atoms. The rather small D values obtained exclude the possibility that we have a molecular radical of the kind Cd-S-Mu, with the electron largely on the Cd atom, since in this case a large anisotropic or dipolar hyperfine interaction would arise, even if the electron density at the muon itself were small or zero. We therefore conclude that the electron wave function is spread out as expected for a shallow donor state. The calculated Bohr radii, assuming a hydrogenic $1s$ electron distribution as the envelope function and scaling the radii with the cube of the ratio of the isotropic hyperfine constants, are also given in Table I. When compared with the values expected from the hydrogenic model, using the effective masses and dielectric constants ϵ of the specific materials,[15] discrepancies are observed, particularly in CdTe. These could reflect details of the local bonding that are not considered in the hydrogenic estimate.

B. Shallow donor level energies

Figure 3 shows the amplitudes of the diamagnetic and paramagnetic fractions of the μSR spectra as a function of temperature. The diamagnetic part is the amplitude of the middle line, and the paramagnetic part is the sum of the amplitudes of the two hyperfine lines, below and above the middle line as seen in Fig. 2. At low temperatures, the paramagnetic fractions dominate for CdS, i.e., almost all muons end up in this state, whereas for CdSe, CdTe, and ZnO the paramagnetic fraction is half the total amplitude or less, and a substantial diamagnetic fraction is present already at low temperatures. Measurements with different CdS samples showed appreciable variations in the formation probabilities of the diamagnetic and paramagnetic states. It

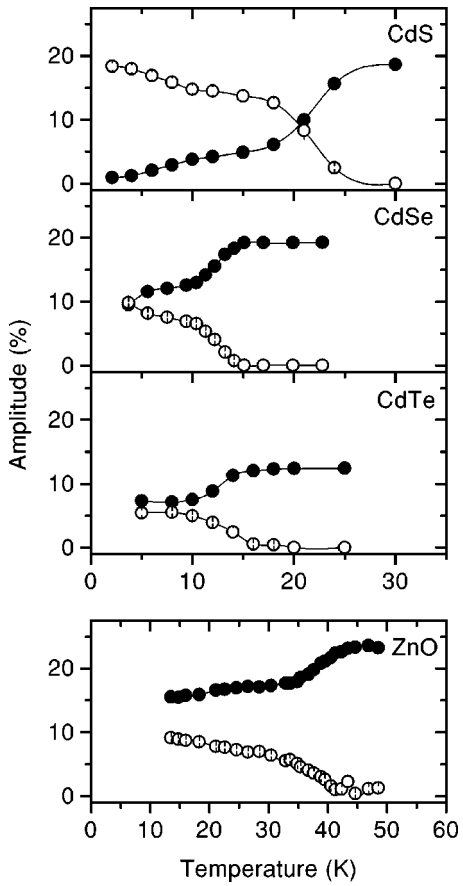

FIG. 3. Amplitudes of the diamagnetic (closed circles) and paramagnetic (open circles) fractions as a function of temperature, derived from fits to the time spectra with three precession lines. The rapid decrease of the paramagnetic amplitude and corresponding increase of the diamagnetic amplitude signals the ionization of the paramagnetic center.

should be noticed also that the paramagnetic fraction decreases at the expense of the diamagnetic fraction with increasing temperature, even below the temperature where the large change of amplitudes is seen in Fig. 3. In CdS, CdSe, and ZnO, all the incoming polarization is accounted for. In CdTe about one-third is lost. This missing fraction is largely recovered in a strong external field (see Sec. III D below). In all four cases, rapid changes of amplitudes are observed in a certain temperature range over which the paramagnetic fraction converts completely to diamagnetic. We relate this conversion to ionization (i.e., dissociation).

For an understanding of this behavior, the last steps in the muon implantation have to be considered in some detail. We would like to distinguish two stages in the muon stopping process, an intermediate epithermal and a final thermal stage. In the epithermal stage there is a loss and gain of electrons by the muon, i.e., an exchange of electrons with the matrix, in particular with the donor and acceptor states. At the transition from the epithermal to the thermal stage, the muon ends up either with or without an electron (in rare cases with two electrons), and this situation determines whether the paramagnetic or diamagnetic fraction is formed at low temperatures. The partition into these fractions can depend on temperature and doping level, thus explaining the slight variation of the fractions at low temperatures as well as the different fractions found in various CdS samples.

The rapid change of the fractions (Fig. 3) at somewhat higher temperatures and the complete conversion to the diamagnetic fraction is due to a different process. We associate it with the ionization of the muonium center in the final thermal stage.

For a quantitative analysis, some further assumptions have to be made concerning the Fermi energy. In thermodynamical equilibrium the chemical Fermi energy is determined by the donor and acceptor states present in the sample and the temperature. One might assume that this is the relevant energy as far as ionization of muonium is concerned. However, within the lifetime of the muon it seems unlikely that full equilibrium will be achieved until well above the ionization temperature. A more realistic assumption might be that after it is stopped, the muon sits in an essentially isolated environment with no dopants in its immediate neighborhood, say in a sphere of radius comparable to the Bohr radius of the shallow donor. With the additional assumption of ''local'' thermodynamical equilibrium, the normal expression for the free-carrier concentration n, in a semiconductor containing N_D donors and N_A acceptors ($N_D > N_A$), can be applied:[16]

$$\frac{n(n+N_A)}{N_D-N_A-n}=\frac{N_c}{2}\exp\left(-\frac{E_D}{kT}\right), \tag{3.3}$$

where N_C is the effective density of states in the conduction band and the factor 2 accounts for the level degeneracy. In our case, N_D is identified with the concentration of muonium centers and N_A is set equal to zero, assuming that no other acceptors or donors besides the muonium are present in the small volume around the muon. The quantity n is identified with the concentration of ionized (diamagnetic) muonium centers. Equation (3.3) can then be written as

$$\frac{x^2}{1-x}T^{-3/2}=\text{const}\times\exp\left(-\frac{E_D}{kT}\right), \tag{3.4}$$

where $x=n/N_D$ is the fraction of ionized muonium centers and the explicit $T^{3/2}$ dependence of N_C on temperature has been taken into account. The quantity $[x^2/(1-x)]T^{-3/2}$, with x derived from the change of the diamagnetic fraction, is shown in Fig. 4 on Arrhenius plots. The fit parameter E_D and the temperatures at which the rapid change occurs (midpoint) are summarized in Table II for the four materials studied. Similar results are obtained by considering the change of the paramagnetic fraction. The value of E_D for CdS is changed from that presented earlier,[5] by reanalyzing the data using Eq. (3.4). Also given in Table II are the calculated binding energies derived from hydrogenic formula using effective masses and dielectric constants of the materials.[15] These follow a similar trend to the experimental values.

The parameter E_D in Eq. (3.4) is effectively twice the activation energy for dissociation. If the assumption of thermodynamic equilibrium is not valid for muonium centers, the donor depths in Table II should be halved.

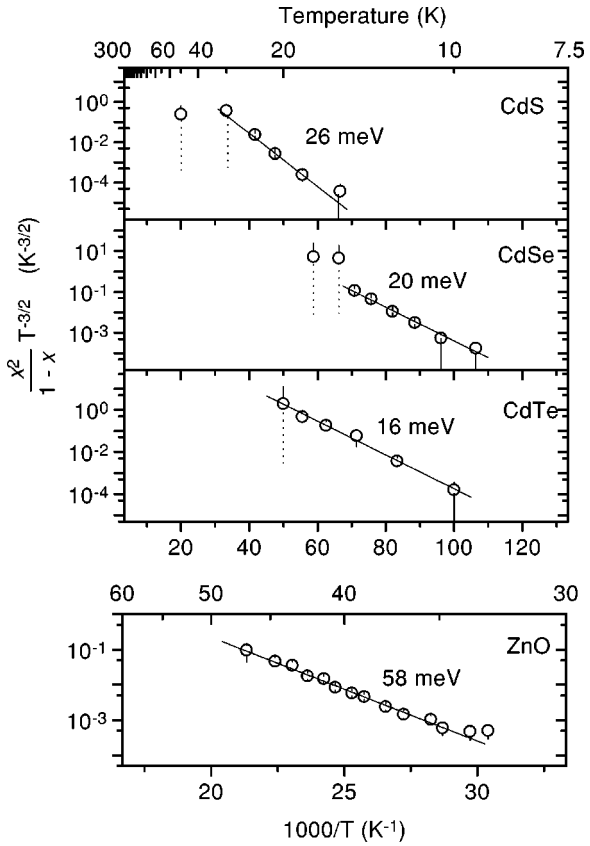

FIG. 4. The quantity $[x^2/(1-x)]T^{-3/2}$, where x is the fraction of ionized donors, as a function of the inverse temperature, for CdS, CdSe, CdTe, and ZnO. The level energies derived from these plots are shown in the figure and in Table 2. The dashed lines in the error bars indicate that the corresponding standard deviation exceeds the plot range.

C. Muon site and diffusion

Site determinations can be made by comparing the linewidth of the diamagnetic signal with the linewidth calculated from the rms magnetic-field distribution created by the nuclear magnetic dipoles around the muon. For this purpose we measured the Gaussian depolarization rate σ (which corresponds to the linewidth) of the diamagnetic fraction above the ionization temperature for CdS (Fig. 5), and compared it with the calculated values assuming different sites in the lattice (Fig. 6). The comparison is made for the 210 K values (which are representative for the temperature regime above

TABLE II. Ionization temperature $T_{\text{ionization}}$ (midpoint of the amplitude of the paramagnetic fraction) and donor level energies E_D^{exp} for CdS, CdSe, CdTe, and ZnO. The donor level energies E_D^{theo}, calculated in the hydrogenic model with the effective masses and dielectric constants of the individual materials are shown (Ref. 15).

	CdS	CdSe	CdTe	ZnO
$T_{\text{ionization}}$ (K)	22(2)	12(2)	13(2)	38(2)
E_D^{exp} (meV)	26(6)	20(4)	16(4)	58(6)
E_D^{theo} (meV)	33	19	11	52

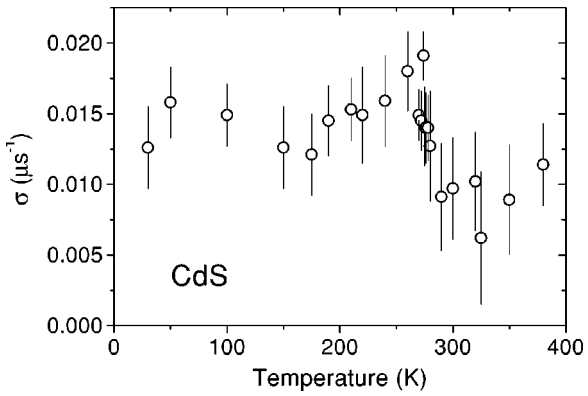

FIG. 5. Depolarization rate σ, derived from the time spectra with the standard Gaussian depolarization function, as a function of temperature, for the dissociated state in CdS.

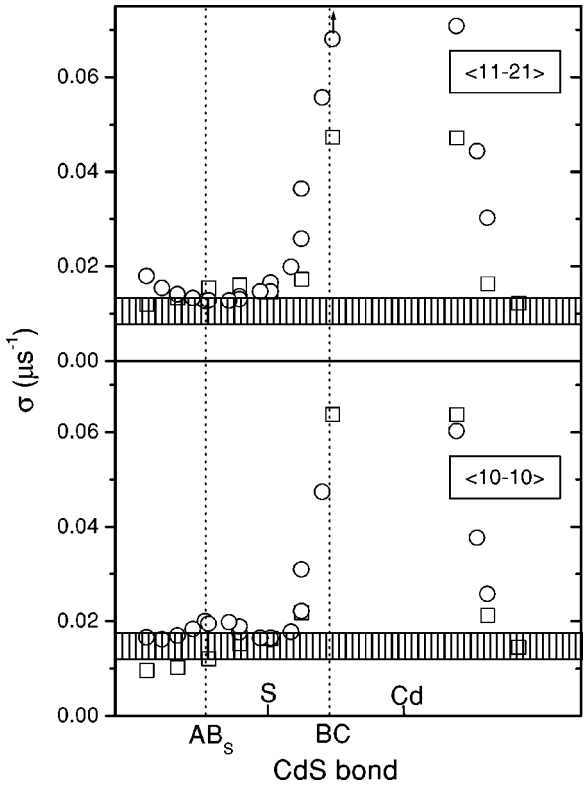

FIG. 6. Experimental depolarization rates σ (shaded areas) for CdS at 210 K, for two orientations of the crystal with respect to the external field, compared to theoretical calculated values (open symbols). On the lower frame the data for the $\langle 10\bar{1}0 \rangle$ and on the upper frame for the $\langle 11\bar{2}1 \rangle$ orientation are shown. The σ values associated with the nuclear magnetic moments of the odd-spin Cd isotopes were calculated along the bond directions, i.e., along the c axis (open squares) and along the three bonds at approximately 109.4° to the c axis (open circles). At the abscissa, the position of the S and Cd atoms are indicated together with the position of the antibonding (AB_S) and the bond-center (BC) sites. The arrow near the BC site indicates that the value exceeds the maximum value of the vertical scale. The dashed-area represents the range of the experimental values.

the ionization threshold but below the temperature at which diffusion or other dynamics sets in; see below) obtained for two orientations of the single-crystal sample: $\langle 11\bar{2}1\rangle$ or $\langle 10\bar{1}0\rangle$ parallel to the external field. Owing to the low abundance of the isotopes ^{111}Cd and ^{113}Cd, which are those with nonzero nuclear moments, the measured widths are very low and almost at the limit of the experimental detectability, yielding large errors.

The calculations were made separately for the four possible bond directions, i.e., along the *c* axis or along the three bonds at 109.4° to the *c* axis. The σ values for these nonequivalent directions are slightly different. If the population probability of on-axis and off-axis sites were similar, a weighted average would have to be taken but this is not necessarily the case and the conclusions do not depend on this assumption. Good agreement, also concerning the tendency in the angular dependence, is obtained assuming the muonium site is close to the antibonding site near the anion (AB_S). The predicted values for the bond-center site are not consistent with the experiment even if a moderate elongation of the bond is assumed. Thus, unless there is a site change or electron capture, the antibonding site is the most probable position for the paramagnetic center of CdS. The antibonding site was found also in our previous work on chalcopyrites,[7] which have similar properties to the II−VI compounds studied here.

Motional narrowing in CdS is clearly seen in Fig. 5 in the temperature range between 260 and 300 K. With the large error bars of the present data, an Arrhenius plot does not give reliable results; thus we rather used the temperature at which motional narrowing occurs to compare with other systems. Motional narrowing has been observed at similar temperatures in the chalcopyrite compounds,[7] and, for these, activation energies around 220 meV have been deduced. A similar value can be assumed for the muon motion in CdS on the basis of the similarity mentioned above.

D. Deep-level "normal" muonium

In CdTe a missing fraction is present at all temperatures in transverse-field spectra recorded below 300 K (see Fig. 1). In fact, the sum of the asymmetries of all muon frequencies amounts only to 11% of the 20% total amplitude in this experimental arrangement.

To obtain further information on the state concealed in this missing fraction, a decoupling experiment in longitudinal field was performed at 4.5 K. In Fig. 7 we plot the measured polarization after subtraction of the diamagnetic fraction (the latter measured in transverse field). If complete recovery occurred, the polarization would go from 0 to 1 in this plot. It can be seen that an abrupt decoupling occurs at very low fields. This recovery is due to the shallow muonium state known from the transverse-field experiments. A far more gradual recovery occurs for higher fields, but even at 0.45 T the polarization is not fully recovered. The remaining missing fraction of approximately 10% is possibly due to a muonium state with a fast electron-spin fluctuation.

The gradual recovery seen in Fig. 7 corresponds to the decoupling of a hyperfine interaction constant of 2400 $\pm$400 MHz. This is about half of the value for free atomic muonium (4463 MHz), and is of the same order of magnitude as for "normal" muonium in Si and Ge. No signs of anisotropy are seen in this repolarization curve. Thus a so-called "normal" muonium—a deep-level state—exists in CdTe. This is formed on implantation with a probability of approximately 38%, to be compared with 25% for the shallow state. No indication of such a "normal" muonium state was found in the other three cadmium compounds, which have hexagonal structure, whereas CdTe is cubic.

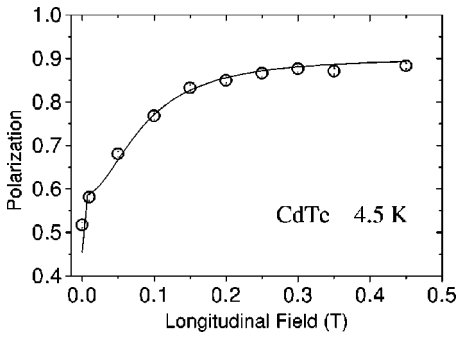

FIG. 7. Longitudinal-field repolarization curve for CdTe at 4.5 K, showing the fraction of the polarization due to the paramagnetic components. The total amplitude expected for all muons minus the diamagnetic fraction seen in transverse field gives the normalization for this plot. The sharp low-field recovery is the decoupling of the shallow-level muonium and the more gradual recovery is the decoupling of a "normal" muonium state with hyperfine constant $A = 2400(400)$ MHz. Full recovery is not achieved up to 0.45 T.

E. Zn chalcogenides

We have also investigated the compounds ZnS, ZnSe, and ZnTe. In a transverse field, we observed a diamagnetic fraction of the order of 3–10% and, in ZnS and ZnSe, the already known "normal" muonium oscillations,[2] with a fraction of about 15–25%. The remaining fraction (70–90%) is missing in the transverse field. In longitudinal-field decoupling experiments, most of this missing part is repolarized at a value of the field corresponding to a hyperfine constant of the "normal" muonium type, i.e., a large fraction of the free-muonium value. However, a small fraction remained unpolarizable and only at very high fields, larger than 2 T, a fast decaying signal appeared, indicating that a fast relaxation process is acting on this state and that the relaxation can be suppressed only at these high fields. In the Zn chalcogenides no indication of a paramagnetic fraction related to the shallow donor state, observed in the Cd chalcogenides and in ZnO, could be seen.

IV. UNIFIED SET OF RULES

We propose here a general set of rules to characterize the muon states in tetrahedrally bonded semiconductors. It combines the various models and ideas put forward in the literature for specific materials or for special aspects of this field.[2–4,8,9,11] It is not intended to give quantitative values for energies, etc., but rather a framework for the interpretation and understanding of the data.

Rule 1: The thermodynamically stable states are Mu^+ in *p*-type material and Mu^- ($\mu^+e^-e^-$) in *n*-type material. This is known as the negative-*U* behavior of hydrogen in this class of materials. (We use the chemical nomeclature Mu^+ and Mu^- here, these states mimicking H^+ and H^-, reserving Greek μ^+ for the incoming muon before chemical association with the host.)

Rule 2: The positive-ion Mu^+ traps either at the bond center in covalently bonded materials (Si, Ge, GaAs, etc., where it is attracted to the high density of spin-paired bonding electrons) or at the antibonding site, close to the anion, in more ionically bonded materials (CdS, GaN, etc.). The negative ion Mu^- is nonbonding and sits at an open interstitial site, at the tetrahedral interstitial site in cubic materials or at the corresponding site in hexagonal crystals. In compound cubic semiconductors, Mu^- prefers the cation cage and avoids the anion cage.

Rule 3: The implanted muon often comes to rest with just one electron associated with it, but thermalization with no electron and in rare cases with two electrons are also possible. At low temperatures and low dopings, charge and site changes may be hindered and a variety of metastable states may be formed, in particular the neutral centers (paramagnetic muonium) with just one electron bound to the muon. Potential barriers between the different configurations control the relative thermal stabilities, site changes, and mobility.

Rule 4: Neutral muonium ($Mu^0=\mu^+e^-$) related to the unbound Mu^- but missing one electron, is a deep center and the hyperfine interaction constant is of the order of the vacuum value. The muonium center originating from bound Mu^+ is either shallow (example: shallow donor as in CdS) or medium deep (example: bond-center muonium in Si). We suggest—although the general validity is by no means confirmed—that the donor is shallow if the muon is at the antibonding site and medium deep if the muon is at the bond center.

Rule 5: Spin-exchange scattering with charge carriers is superimposed on the charge and site changes. Spin exchange becomes increasingly important with increasing temperature and doping.

V. DISCUSSION

We first give a short account of what is expected in this model for the well-known case of Si and then come to a detailed discussion of the compounds studied in this work.

In Si the muon thermalizes in most cases with one bound electron (rule 3). As a result of local fluctuations or residual kinetic energy at the end of their path, some muons end up as muonium at bond centers, the others as muonium at the tetrahedral interstitial sites. After the formation of these centers, conversion between these sites is hindered by a barrier. From these initial configurations a rich variety of conversions to other states takes place depending on temperature and doping.

In CdS, the major fraction of muons forms the shallow donor state discussed in this paper. The diamagnetic fraction observed at low temperatures probably represents muons at the same site as the shallow donor state but without the electron, either because the muon brought no electron with it or because the electron was lost in the final deexcitation steps after the muon stopped.

In CdSe the formation probabilities of the diamagnetic and paramagnetic states at low temperatures are almost the same. We assume that again in this case only bound muons at the antibonding site are formed, half of them having an electron and half not. In principle, part of the diamagnetic fraction could be due to Mu^-. However, in undoped materials and at low temperatures the formation of this configuration is unlikely due to the lack of sufficient electrons. It is noteworthy that the hyperfine interaction constant is a factor of three smaller than that in the other Cd compounds. Possibly the contact hyperfine interaction is composed of two contributions, one from the electron density directly around the muon and the other from electrons at the Cd sites with their distributions reaching the muon site in their tails. Slight variations in the crystal structure and electronic properties could give rise to large variations of the actual electron spin-density distribution at the muon site, thus resulting in variations of the hyperfine parameters.

In CdTe, four components can be identified. The diamagnetic and the paramagnetic components seen at low temperature in transverse fields have similar formation probabilities, accounting for about 30% and 25% of the incoming muons. Within the remaining 45% whose polarization is invisible in transverse-field spectra, about 38% can be attributed to ''normal'' muonium type centers, recovered in a longitudinal-field decoupling experiment, as discussed in Secs. III and IV. The still remaining 7% missing fraction probably arises from centers with a large hyperfine constant and a fast-electron spin relaxation, which cannot be decoupled with the fields applied here. The paramagnetic and the diamagnetic part seen in transverse field are attributed again to the shallow donor center, with and without an electron, as discussed above for the other Cd compounds. CdTe is therefore remarkable—and so far unique—in showing the coexistence of deep and shallow states. We suggest that this difference with the other two Cd compounds is related to the fact that CdTe is cubic, whereas CdS and CdSe are hexagonal. In the cubic case, it seems likely that the neutral trapped atom is stabilized in the tetrahedral metal-ion cage for which there is no precise equivalent in the hexagonal lattice and that a site change towards the antibonding site is hindered by a barrier. In the hexagonal structure, no such cage hindrance is present. We do not have much information on the fast relaxing component and can only speculate on its nature. It seems likely that it is the same ''normal'' type of muonium as is responsible for the deep state, but in a local environment, e.g., defects and grain boundaries, where fast electron exchange takes place.

In ZnO, the diamagnetic and paramagnetic components account for the full polarization of the incoming muons. Both components are attributed to the shallow muonium center, one with the bound electron, the other without it, as discussed above. Here the fraction with no electron is rather large. The hyperfine interaction constant and the electron binding energy are appreciably larger than in the Cd com-

pounds, but this tendency is expected from the effective mass theory, considering the material parameters.

The 3–10 % fraction of diamagnetic muons in the Zn chalcogenides could be due to this shallow donor configuration without the electron captured, but we have no experimental confirmation of this.

VI. CONCLUSIONS

The μSR data show clear evidence for the formation of a shallow donor muonium center in the Cd chalcogenides and in ZnO. Because of the similarity in the electronic properties of the muon and the proton, and also because a shallow donor hydrogen center has been predicted theoretically for ZnO, the existence of the corresponding hydrogen center in these materials can be inferred. The small diamagnetic fraction of 3–10 % could be due to this shallow donor center without the electron, but this is not yet clear. In the corresponding Zn chalcogenides, ''normal'' muonium centers corresponding to deep states are seen. So far, the coexistence of the deep and shallow centers has only been established for CdTe. It seems that in the Cd chalcogenides and in ZnO, the formation of the shallow center or states derived from it are dominant, whereas in the Zn chalcogenides the formation of the Mu^- related states are preferred. These findings should carry over in large degree as a guide to the states and electrical activity of interstitial hydrogen, impacting doping issues in these materials.

ACKNOWLEDGMENTS

We thank J. Pinto da Cunha for his computer code of the Lomb method, and J. A. Paixão, A. Matos Beja, and Manuela Silva for x-ray sample orientations. This work was partially supported by PRAXIS XXI (Portugal PCEX/P/FIS/16/96), FCT funding, by EPSRC (GR/R25361), and the European Community through its ''Access to Research Infrastructure action of the Improving Human Potential Program'' (research at ISIS).

[1] *Hydrogen in Semiconductors and Metals*, edited by N. H. Nickel, W. B. Jackson, and R. C. Bowman, MRS Symposia Proceedings No. 513 (Materials Research Society, Pittsburgh, 1998).

[2] B. D. Patterson, Rev. Mod. Phys. **60**, 69 (1988).

[3] S. F. J. Cox and R. L. Lichti, J. Alloys Compd. **253-254**, 414 (1997).

[4] K. H. Chow, B. Hitti, and R. F. Kiefl, in *Identification of Defects in Semiconductors*, edited by M. Stavola, Semiconductors and Semimetals, Vol. 51A (Academic, New York, 1998), pp. 137–207.

[5] J. M. Gil, H. V. Alberto, R. C. Vilão, J. Piroto Duarte, P. J. Mendes, L. P. Ferreira, N. Ayres de Campos, A. Weidinger, J. Krauser, Ch. Niedermayer, and S. F. J. Cox, Phys. Rev. Lett. **83**, 5294 (1999).

[6] S. F. J. Cox, E. A. Davis, S. P. Cottrell, P. J. C. King, J. S. Lord, J. M. Gil, H. V. Alberto, R. C. Vilão, J. Piroto Duarte, N. Ayres de Campos, A. Weidinger, R. L. Lichti, and S. J. C. Irvine, Phys. Rev. Lett. **86**, 2601 (2001).

[7] J. M. Gil, P. J. Mendes, L. P. Ferreira, H. V. Alberto, R. C. Vilão, N. Ayres de Campos, A. Weidinger, Y. Tomm, Ch. Niedermayer,M. V. Yakushev, R. D. Tomlinson, S. P. Cottrell, and S. F. J. Cox, Phys. Rev. B **59**, 1912 (1999).

[8] C. G. Van de Walle, Phys. Rev. Lett. **85**, 1012 (2000).

[9] R. L. Lichti, Philos. Trans. R. Soc. London, Ser. A **350**, 323 (1995).

[10] B. B. Nielsen, K. B. Nielsen, and J. R. Byberg, Mater. Res. Forum **143-147**, 909 (1994).

[11] J. Neugebauer and C. G. Van de Walle, Phys. Rev. Lett. **75**, 4452 (1995).

[12] G. H. Eaton, C. A. Scott, and W. G. Williams, in *Proceedings of the International Workshop on Low Energy Muon Science: LEMS'93*, Los Alamos National Laboratory Technical Report No. LA-12698-C, Santa Fe, NM, 1993, edited by M. Leon (LANL, Los Alamos, 1993).

[13] R. Abela, A. Amato, C. Baines, X. Donath, R. Erne, D. C. George, D. Herlach, G. Irminger, I. D. Reid, D. Renker, G. Solt, D. Suhi, M. Werner, and U. Zimmermann, Hyperfine Interact. **120-121**, 575 (1999).

[14] N. R. Lomb, Astrophys. Space Sci. **39**, 447 (1976).

[15] Landolt-Börnstein, *Numerical Data and Functional Relationships in Science and Technology*, edited by O. Madelung, M. Schulz, and H. Weiss, New Series, Group III, Vol. 17, Pt. b (Springer-Verlag, Berlin, 1982).

[16] K. Seeger, *Semiconductor Physics, an Introduction*, 3rd ed., Springer Series in Solid-State Sciences, Vol. 40, p. 40 (Springer, Berlin, 1985).